Journal of
Manufacturing and Materials Processing

MDPI

Article

Theoretical Manufacturing and Mathematical Analysis of the Spiroid Worm Grinding Process Based on a Solution to the Lead and Angular Velocity Fluctuation Problem Using Lead Angle Correction

Sándor Bodzás [1,*], Gyöngyi Szanyi [2] and Tatjana Lazovic [3]

[1] Department of Mechanical Engineering, University of Debrecen, Ótemető Str. 2-4, 4028 Debrecen, Hungary
[2] Department of Basic Technical Studies, University of Debrecen, Ótemető Str. 2-4, 4028 Debrecen, Hungary; szanyi.gyongyi@eng.unideb.hu
[3] Department of Machine Design, University of Belgrade, Kraljice Marije 16, 11120 Belgrade, Serbia; tlazovic@mas.bg.ac.rs
* Correspondence: bodzassandor@eng.unideb.hu

Abstract

The present study provides a comprehensive analysis of the grinding process of spiroid worm shafts, focusing on the combined application of lathe center displacement and lead angle correction on a conventional cylindrical grinding machine. The objective is to generate accurate tooth profiles for spiroid worms and spiroid hobs while minimizing lead errors and angular velocity fluctuations inherent in the worm grinding process. The implementation of lathe center displacement alters the kinematics of the workpiece, transforming the nominal circular path into an elliptical path. This kinematic modification introduces manufacturing deviations due to the continuously varying radius along the elliptical path. To address these effects, a novel mathematical model is developed, enabling the determination of an optimal grinding wheel profile for both spiroid worms and hobs under these non-ideal motion conditions. The simultaneous application of the optimized grinding wheel profile and lead angle correction is shown to significantly enhance the profile accuracy of the generated tooth geometry. Furthermore, a detailed manufacturing analysis is carried out to investigate the influence of variations in the half-taper angle on key process parameters. Based on the analytical and computational results, a methodological solution is proposed to effectively mitigate lead errors and angular velocity fluctuations in spiroid worm grinding.

Keywords: spiroid; lead; angular velocity; lathe center displacement; driving pin

Academic Editor: Steven Y. Liang

Received: 11 April 2026
Revised: 29 April 2026
Accepted: 30 April 2026
Published: 7 May 2026

1. Introduction

Spiroid worm face gear-paired spiroid worm gear drive (Figure 1) is usable as the backlash-free drive of robots, an advantageous working machine, since the backlash-free drive can be provided simply based on the axial adjustment of the spiroid worm. This gear drive can provide higher torque transmission and better load. The center distance is smaller than in a cylindrical worm gear drive. It can be used with lower noise. Higher efficiency and lower heat development are available. It is a self-locking gearbox.

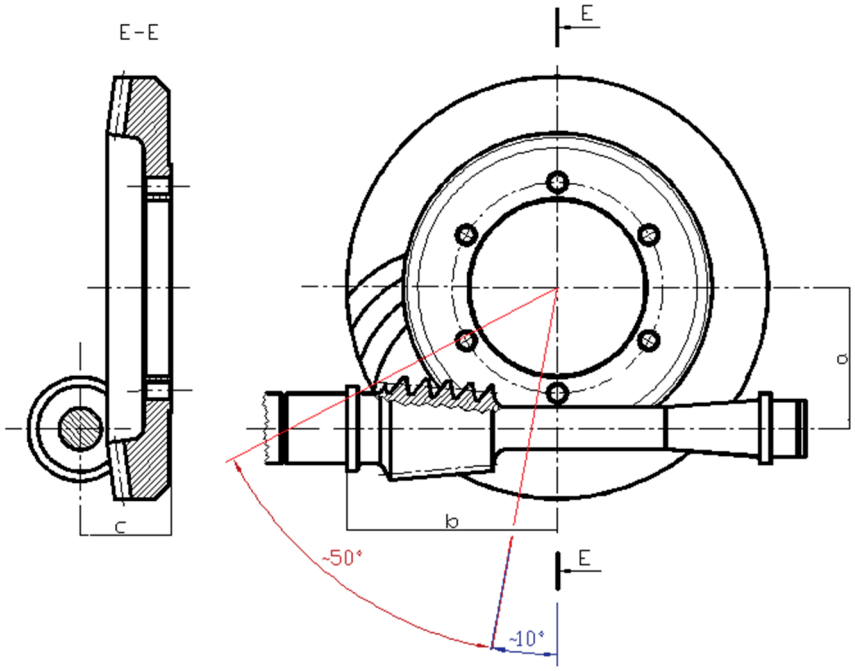

Figure 1. The location area of the spiroid worm compared to the face gear in a top view.

The research can be classified as applied research, as it is aimed at achieving a specific industrial objective, namely the development of a new manufacturing technology. The feasibility of the proposed technology is substantiated through theoretical methods, including analytical calculations, modeling, and simulation. Due to the lack of necessary equipment and resources, practical validation, prototype development, and experimental investigations are not carried out; therefore, the research remains at an early, theoretical stage of the development process.

To better understand the challenges outlined above, it is essential to review the existing body of research related to spiroid worm manufacturing and grinding processes.

The work in [1] shows the theorem and the construction of spiroid worm gear drives. It defines the differences among the various types of gear drives that use a face gear. It explains in detail the roles of the worm design process, including the shape of the teeth, load capacity, motion velocity, etc. It also gives advice on when it is worth using this spiroid gear drive. The pinion taper angle, $\delta 1$, may vary between 0 and 10 degrees [1].

The work in [2] shows the theorem, the application, and the manufacturing processes of different types of worm gear drives. A complex mathematical model is developed that allows different types of worm gear drives and their manufacturing processes to be analyzed. Grinding technologies have also been developed for both the spiroid worm and the hob [2].

The work in [3] shows that new geometric models and calculation methods developed during the research enable better fit, reduced backlash, and higher efficiency of drive pairs, while also accounting for manufacturing technology limitations. The work focuses on integrating manufacturing and design, i.e., optimizing the geometry and operation of drive pairs using computer-aided design (CAD/CAM). Overall, the work aims to develop the design and manufacturing of drivetrains on a scientific basis, with a complex approach ranging from geometry to manufacturing technology [3].

The work in [4] shows a developed spiroid grinding technology, where lead angle correction and changes in center distance are used together to enhance the accuracy of the spiroid worm. Since the center distance is changing, the spiroid worm has not adjusted its

half-taper angle. The solution of the modeling process of the face gear connecting to the spiroid worm is also determined in this work [4].

The work in [5] is a patent that is registered to Dudás I., Bodzás S., Dudás I. Sz., and Mándy Z. It describes the design of a spiroid worm gear pair with a concave thread profile. The solution aims to increase the load capacity, efficiency, and accuracy of the gear pair while reducing wear. In addition, the patent details a process for producing concave-profile worms by grinding, enabling the production of precision, geometrically optimized worm gears in an industrial environment. Overall, the patent aims to improve the geometry and manufacturing of worm gears to enhance the gear pair's mechanical and operational properties [5].

The work in [6] addresses the development of spiroid worm gears, with a particular focus on the use of a concave thread profile in the axial section, which improves the load capacity, efficiency, and service life of the drive pair. The paper presents a new manufacturing technology that uses a lathe center displacement to manufacture gears with precision and optimized geometry. The results improve the mechanical performance of worm gears, reduce wear, and increase production efficiency [6].

The work in [7] analyses grinding processes and technological settings of the helical surface as follows: the helical shaft is ground by adjusting the half-taper angle, so that the axial distance between the screw and the grinding wheel remains constant throughout the entire operation. This adjustment causes variable angular velocity in the screw's rotation at a constant wheel speed, affecting the accuracy of the thread pitch and thread profile during grinding. The study therefore analyses how geometric and setting parameters affect grinding accuracy and quality in the production of spiroid screw shafts, a process performed on a conventional grinding machine [7].

The work in [8] investigates the application of intelligent, computer-controlled manufacturing systems in the production of helical surfaces (e.g., screws and threaded parts), with a focus on geometrically correct and precise machining. The aim of this work is to replace traditional manufacturing methods with optimized, automated systems that ensure accurate geometric profiles, proper fit, and reduced backlash, while increasing productivity and reducing the possibility of errors. The dissertation combines geometric modeling, simulation, and manufacturing technology processes, thus offering a complex, industrially applicable method for the manufacturing of precision screw surfaces [8].

The work in [9] is a candidate's dissertation that examines the problems of manufacturing geometric design of mechanical surface pairs, such as gears and pulleys. The focus of the work is on how to ensure accurate fit and proper surface contact during manufacturing using the reach model. The aim is to reduce manufacturing errors, increase accuracy, and optimize the mechanical performance of surface pairs [9].

The work in [10] discusses the basic characteristics and operation of spiroid worm drives. The work presents the geometry, transmission mechanism, load capacity, and wear behavior of the spiroid drive, as well as its advantageous properties compared to conventional worm drives, such as higher efficiency and compact size. The article provides an important early overview of the design, application, and operating parameters of spiroid drives, highlighting their role in precision industrial drives [10].

The work in [11] is a comprehensive, practice-oriented handbook on the design and manufacture of gears. It presents the geometric foundations of gears, including spiroid worm gearing, load and strength calculations, and the operation of various gear types. It discusses in detail manufacturing technologies; heat treatment; accuracy and quality control; and noise, vibration, and wear-reduction methods. The aim of the work is to transform theoretical knowledge into applicable engineering solutions through industrial examples [11].

The work in [12] is a fundamental work in gear theory that provides a detailed mathematical and geometric description of teeth. It presents in detail the theory of engagement; involute and non-involute teeth; and the geometric modeling of cylindrical and spiroid worms, and hypoid gears. It places special emphasis on tooth surface generation, the effects of errors and modifications, and computer-aided design methods. The book primarily provides a theoretical basis for researchers and development engineers, while also laying the foundation for practical design [12].

The work in [13] summarizes the most important results of modern gear research and design. It discusses the geometry of conventional (known wheelbase) and unconventional gears (special gear and wheelbase), the theory of engagement, and the design issues of high-precision and high-load drives. It presents in detail computer-aided gear design, tooth surface modeling, load distribution, and dynamic behavior analysis. The book is primarily intended for researchers and advanced design engineers seeking deeper theoretical and modern engineering approaches in gear technology [13].

The work in [14] covers the theoretical and practical aspects of gear drives, paying tribute to F. L. Litvin, a pioneer of modern gear theory. The book discusses in detail the geometric and kinematic models of gears, the theory of engagement, the analysis of load distribution, and tooth surface interactions. In addition to traditional cylindrical and bevel gears, it also presents the design aspects of special drives, such as helical, hypoid, and worm gears. This work places great emphasis on modern computer design, simulation and optimization, including the study of dynamic behavior, noise and vibration reduction, and wear and fatigue. The collection of study formats allows the reader to get acquainted with the various research directions and practical applications of gear technology, making the book a valuable resource for researchers, development engineers, and advanced mechanical engineering students alike [14].

The work in [15] reviews the development directions of the theory and practice of spiroid gears in the research environment of Kalashnikov ISTU over the past twenty years. The developments cover the theory of gears and gear design methods, new and improved gear types, competitive gear layouts, and efficient manufacturing technologies. A prominent role was given to computer-aided design, in particular, the SPDIAL+ software (Based on the article, it cannot be determined which version of SPDIAL+ was used.), which enables detailed examination of gear engagements, consideration of defects and deformations, and optimization tailored to real operating conditions. The main area of application of the developments is the operation of low-speed, high-load drives, especially pipeline valves, as illustrated by examples [15].

The work in [16] discusses the production of spiroid gears, which can be an alternative to bevel gears and hypoid gears, especially for gear ratios below 10 (often below 6). The main challenge in production is the production of multi-threaded screws and cutters. The study presents solutions for both small series and mass production: for the former, the development of traditional methods, and for the latter, efficient machining processes that can be used on conventional lathes with minor modifications. Numerical examples illustrate how hypoid gears in trucks and trams can be replaced with spiroid gears, with the same or modified installation dimensions. The text highlights that by choosing appropriate geometric and machine-setting parameters, the drive's operation, the contact zone location, and the tool parameters can be effectively controlled [16].

The work in [17] presents the application of multi-tooth, assembled "entry" milling heads for the production of gears. These milling heads are capable of forming helical surfaces with constant or variable pitch, using industrial carbide inserts, or in special cases, multi-blade disposable inserts. The study discusses mathematical models for calculating and evaluating the generation parameters, surfaces, and the possibilities and limitations

of parameter selection. It also presents the basics of tool design and machine setup, as well as the practical application of the method in small- and large-series production for spiroid and cylindrical worm drives (single- and multi-thread) and bevel gears with helical tooth profiles. The novelty of the technology is that it offers an economical and efficient alternative to traditional manufacturing methods [17].

The work in [18] provides information on the manufacturing technology of spiroid cylindrical worms. It describes a method for the analytical calculation of the profile with a disk-shaped grinding wheel, which allows precise grinding of different types of worm surfaces (e.g., Archimedean, convolute, and involute). By applying the calculation methodology, machining of the working side surfaces of hardened worms can be achieved with high accuracy. In addition, the wear of the spiroid face gear during engagement is significantly reduced, which is especially important because the wheel's ring gear is made of bronze. Thus, this technology increases accuracy and reduces part wear during production [18].

Spiroid gears are a reasonable alternative to bevel and hypoid gears in the low-gear-ratio range (about 12 or less). The work in [19] investigated the potential for controlling engagement quality at low gear ratios and quantitatively evaluated how the degree and nature of engagement localization affect tooth contact stresses. It highlighted the advantages of designing a longitudinal contact path and contact pattern. Numerical studies show that changing the geometric parameters affects the main characteristics of the gear: contact stress, sliding velocity, associated force, and efficiency. It is concluded that spiral bevel gears are comparable to bevel and hypoid gears in these properties, although parameter changes have contradictory effects: for example, reducing stress often increases sliding velocity and reduces efficiency. The work also provides a quantitative comparison of the characteristics of the spiroid gear, traditional bevel gears, and hypoid drives [19].

The work in [20] describes the precise, NC-machined design and simulated design of spiroid gears, using two machining methods. Based on kinematic and geometric relationships, a geometric model was developed for tooth design and the determination of the modification depth along the tooth line. The equations of the tooth line and the calculation formulas for the modification depth were calculated, assuming the correct fit of the worm and the spur gear. Using algorithms and mathematical formulas, computer programs were developed to design gears and calculate their geometric dimensions, as well as to visualize the modification depth along the tooth line. The study illustrates the method with simulation results on a specific gear example. Finally, two tooth preparation methods with a single-number cutting tool were presented: an exact and an approximate method. A comparative simulation was also conducted for both using algorithms and programs [20].

The work in [21] provides an overview of the design innovations in worm-type gears developed at the research and development center of the "Institute of Mechanics" in Izhevsk, Russia. The main innovations are spiroid gears with low speed and small ratios, cylindrical worms with hardened steel gears, and planetary spiroid gears. The challenges of series production for low-speed spiroid and cylindrical worm gears include very high loads, consideration of layout constraints, simplification and unification of tools, and multiple ratios in a single design. For small ratios, spiroid gears can be an effective alternative to hypoid and bevel gears, thanks to their favorable tooth engagement and economical manufacturing. Hardened steel worm gears have an advantageous arrangement of tooth engagement lines, which improves lubrication and reduces wear. Two versions were tested [21].

The work in [22] investigates the design of tooth surfaces of two-thread spiroid worm gears with straight-line contact and involute tooth profile. It states that all tooth surfaces are involute helicoids and analyzed in detail how they can be formed. Several methods have been developed for machining tooth surfaces, for example, on a milling machine, on

an NC lathe, or by fly cutting. The involute helicoid is essentially a combination of the motion of a point or a straight line: the rotation of the base cylinder and the parallel motion of the point in the plane give the helical trajectory of the tooth surface. The formation of tooth surfaces can be based on these geometric and kinematic principles, thereby ensuring precise, helical tooth profiles for spiroid drives [22].

Although several studies have addressed various aspects of worm gear manufacturing, the combined effects of lathe center displacement and lead angle correction have not been comprehensively investigated.

This literature review directly motivates the present study, which aims to develop a novel analytical model and methodological solution.

The notation used in the publication can be found in Appendix A.

1.1. Comparative Analysis with Existing Studies

International research in the field of spiroid worm gears is carried out along several main directions. On the one hand, they focus on the development of manufacturing technology and the development of precision grinding processes, which aim to increase the accuracy of tooth profiles and reduce manufacturing errors. On the other hand, the focus is on theoretical modeling and the integration of CAD/CAM systems, enabling the optimized design and simulation of spiroid worm gears. In addition, the study of dynamic behavior and tooth contact is given a prominent role in revealing the effects of tooth engagement on load capacity and operational stability. The analysis of wear and tribological performance is also important, especially from the perspective of material durability and lubrication optimization. Finally, the optimization of tooth geometry allows for better fit, reduced backlash, and more efficient operation of the gears.

1.2. Advantages of the Method Used in This Research

1. Application of a combined method in manufacturing

While previous research has separately investigated manufacturing technology, thread grinding processes, CAD/CAM-based design, or dynamic and tribological studies, this study applies lathe center displacement and lead angle correction together on a conventional cylindrical thread grinding machine. This allows for more accurate production of spiroid worm tooth profiles under real, non-ideal motion conditions.

2. New mathematical model for kinematical investigations

The publication developed a new mathematical model for manufacturing technology that handles manufacturing deviations due to the transition of the workpiece to an elliptical path. This allows the determination of the optimal grinding wheel profile for spiroid worms and hob, which has not been presented in such a specific form in previous studies.

3. Increased accuracy and reduced errors

The method significantly reduces lead and angular velocity fluctuations by simultaneously applying optimized grinding wheel profile and lead angle correction, thus improving the accuracy and reproducibility of tooth profiles. This provides a practical, engineering solution for tight adherence to manufacturing tolerances.

4. Detailed manufacturing analysis

This study analyzes the impact of changes in the half-taper angle on key process parameters, allowing for optimization of manufacturing parameters and prediction of defects. This level of detail complements previous theoretical and industrial reviews of research that have provided more broad but less specific guidance.

5. Methodological contribution

Overall, the research presents a new, practically applicable methodology for optimizing the spiroid worm grinding process, which integrates the treatment of kinematic problems, wheel profile optimization, and lead correction, thus increasing both the accuracy and efficiency of production.

2. Materials and Methods

2.1. Problem of the Adjustment of the Spiroid Worm Using Lathe Center Displacement

The overall grinding process is shown in Figure 2. The spiroid worm adjusts the half-taper angle (δ_1). This adjustment is called lathe center displacement. The driver plate is fixed to the spindle of the grinding machine and can move together. The number of revolutions (n_g) is provided to the spindle from the primary gearbox of the machine, and the angular velocity of the driver plate is [4,5].

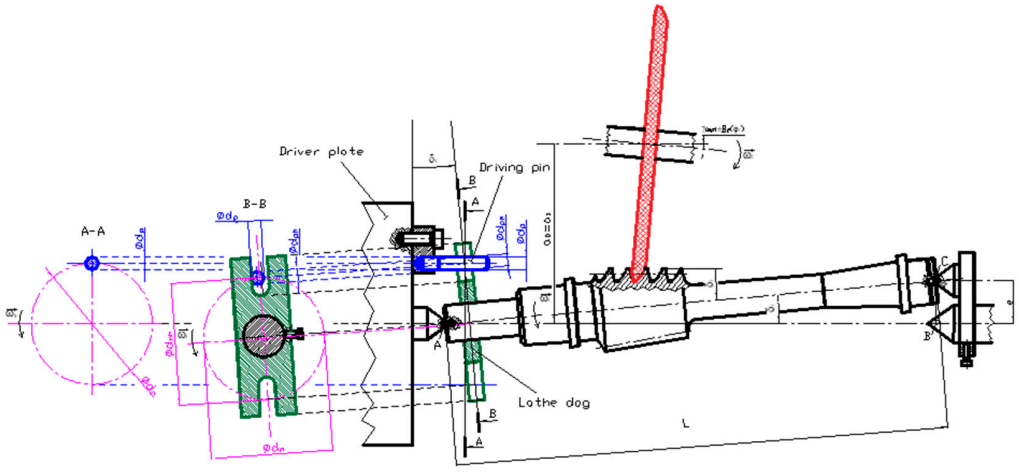

Figure 2. The overall grinding manufacturing process of the spiroid worm shaft.

$$\vec{\omega_g} = 2 \cdot \pi \cdot n_g \tag{1}$$

This ($\vec{\omega_g}$) angular velocity is constant around the d_m diameter, which is the circular path of the driving pin. This element is fixed on the driver plate. The lathe dog is fixed to the adjusted spiroid worm shaft; consequently, its position is also skewed relative to the horizontal. The driving pin and the lathe dog are in contact during the rotation. The rotating lathe dog provides rotation to the spiroid worm shaft.

The circumferential speed of the spindle is [4,5]

$$\vec{v_g} = \vec{\omega_g} \cdot \frac{d_m}{2} \tag{2}$$

The adjustment angle between the lathe dog and the driver plate is also the half-taper angle (δ_1) [4,5]. Due to this δ_1 adjustment, the circular path of the driving pin that belongs to the driver plate is not the same as the path of the driving pin that belongs to the lathe dog (Figure 2). This path is an elliptical path whose minor axis is d_m, but the major axis is [4,5]

$$d_{mh} = \frac{d_m}{cos\delta_1} \tag{3}$$

Since the rotation path of the spiroid worm is an ellipse whose radius is not constant, the $\vec{\omega_1}$ angular velocity of this elliptical path is continuously changing, assuming the same $\vec{v_g}$ circumferential speed on both paths [4,5]:

$$\vec{\omega_1}(\varphi_1) = \frac{\vec{v_g}}{r_e(\varphi_1)} \tag{4}$$

where φ_1 is the angular displacement of the spindle.

During the spiroid worm rotation, the grinding wheel is also rotated ($\vec{\omega_2}$) and angled based on the γ_{opt} optimized lead angle for the optimized grinding wheel peeling station. During the grinding process, the grinding wheel wears, and due to the spiroid geometry, the diameters change, which causes the lead angle to vary along the length of the spiroid worm. Consequently, the real profile of the spiroid worm differs from the theoretical profile [2].

To provide the same worm profile within the prescribed profile tolerance, we must determine the optimized grinding wheel peeling station, as described by Prof. Illés Dudás' principle [2]. It is said that the grinding wheel profiles must be determined at the smallest and largest pitch diameters of the spiroid worm. After that, a middle grinding wheel profile (average) can be determined (optimized profile). Finally, the optimized pitch diameter of the spiroid worm can be determined from the previously calculated optimized grinding wheel profile [2]. Using this optimized grinding wheel profile and the γ_{opt} optimized lead angle calculated at the optimized pitch diameter of the spiroid worm, the spiroid worm can be ground to the prescribed profile tolerance. To enhance profile accuracy, a $\pm B_2$ lead angle correction is also applied simultaneously [3].

During the grinding process, γ_o has to be calculated continuously since the pitch diameter is also continuously changed along the length of the spiroid worm. The formula for the determination of the continuously changing γ_o is the following [4]:

- If $\gamma_{0opt} > \gamma_0$, then

$$-B_2 = \gamma_0 - \gamma_{0opt} \tag{5}$$

- If $\gamma_{0opt} < \gamma_0$, then

$$+B_2 = \gamma_0 - \gamma_{0opt} \tag{6}$$

During the grinding process, the γ_{opt} angle has to be modified based on the current value and sign of the $\pm B_2$ lead angle correction [3,4].

The constant center distance between the spiroid worm and the grinding wheel is [4]

$$a_1 = a_0 = \frac{d_{amax} - p_r \cdot \varphi_1}{2} \cdot cos\delta_1 - h_w + \frac{d_{agw}}{2} + (l + p_a \cdot \varphi_1) \cdot cos\delta_1 \tag{7}$$

The L total shaft length and the δ_1 half-taper angle are known; therefore, the e eccentricity distance is calculatable (ABC triangle, Figure 2) [4]:

$$e = L \cdot sin\delta_1 \tag{8}$$

2.2. Kinematical Analysis of the Driving Pin Mechanism

The kinematical figure of the driving pin mechanism can be seen in Figure 3.

The driving pin is fixed on the driver plate. The A point is the initial contact point of rotation between the driving pin and the lathe dog, where the φ_1 angular displacement of the driver plate is zero. After $\varphi_1 = 180°$ angular displacement, we get the maximum x_{max} contact point displacement on the B point (Figure 3). During one driving pin revolution, the contact points are continuously moving between the A and B points. At the beginning of the rotation, $x = 0$. $x = x_{max}$ is in the case of $\varphi_1 = 180°$. Eventually, $x = 0$ is recovered at the end of one revolution for $\varphi_1 = 360°$ (Figure 3).

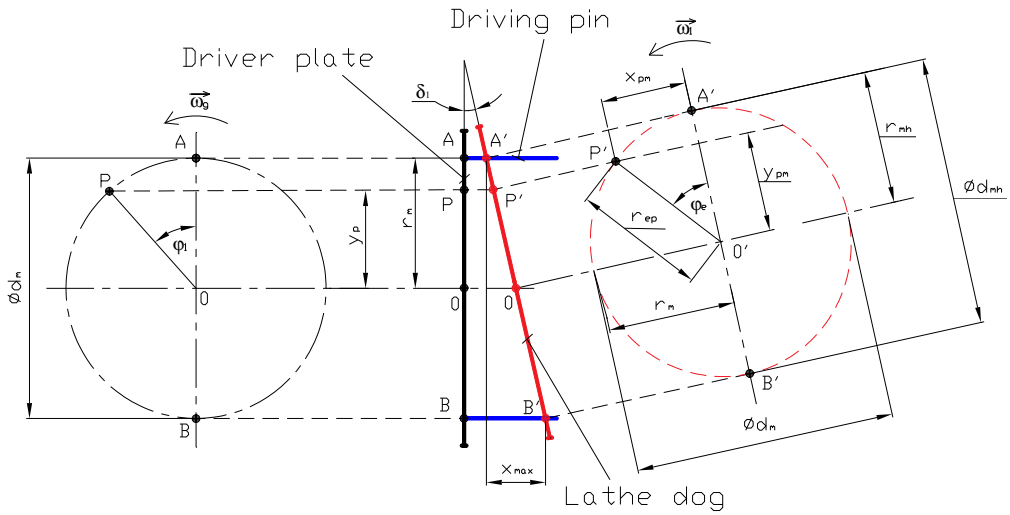

Figure 3. A kinematical figure of the driving pin mechanism.

To analyze the kinematic mechanism (Figure 3), the following initial parameters must be provided: L, n_g, d_p, d_m, and δ_1 [4]. The variable is the φ_1 angular displacement on the circular path that can be changed between 0 and 360°. The x contact point displacement is

$$x(\varphi_1) = (1 - cos\varphi_1) \cdot \frac{d_m}{2} \cdot tan\delta_1 \tag{9}$$

The P point is an arbitrarily selected point on the circular path of the driving pin (Figure 3). It has a concrete angular displacement value φ_1. The distance $\overline{OP}$ is equal to the r_m radius of the circle (Figure 3):

$$r_m = \frac{d_m}{2} \tag{10}$$

The y_p distance is (Figure 3)

$$y_p = r_m \cdot cos\varphi_1 \tag{11}$$

The y_{pm} distance is on the elliptical path (Figure 3):

$$y_{pm} = \frac{y_p}{cos\delta_1} \tag{12}$$

The x_{pm} distance is on the elliptical path (Figure 3):

$$x_{pm} = \sqrt{1 - \frac{y_p^2}{\left(\frac{d_{mh}}{2}\right)^2}} \cdot \frac{d_m}{2} \tag{13}$$

The r_{ep} radius is (Figure 3)

$$r_{ep} = \sqrt{y_{pm}^2 + x_{pm}^2} \tag{14}$$

The φ_e angular displacement that belongs to the P′ point on the elliptical path is (Figure 3)

$$\varphi_e = sin^{-1}\left(\frac{x_{pm}}{r_{ep}}\right) \tag{15}$$

The φ_e angular displacement on the elliptical path can be determined directly based on the φ_1 angular displacement on the circular path using the following formula:

$$\varphi_e(\varphi_1) = sin^{-1}\left(\sqrt{1 - \frac{cos^2\varphi_1}{cos^2\delta_1}}\right) \tag{16}$$

All in all, if an arbitrarily selected point is given on the circular path, the projection of this point (the corresponding point of the arbitrarily selected point) on the elliptical path can be determined based on (11)–(16).

In order to determine the lead error and the angular velocity fluctuation, the function between φ_1 and φ_e is necessary. Knowing this correlation, a further manufacturing analysis can be performed in the following steps.

2.3. Solution of the Lead Error and Angular Velocity Fluctuation Problems

The circular and elliptical paths are shown together in Figure 4. Due to the half-taper adjustment, the initial circular path is modified to an elliptical path, leading to changes in the angular velocity and the lead error of the thread during the grinding process, which can cause quality errors on the workpiece [4,5].

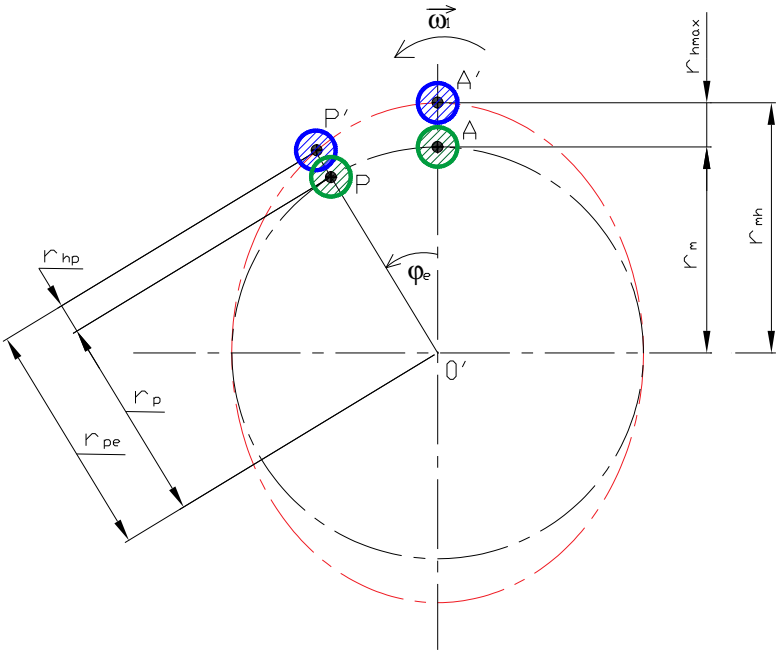

Figure 4. The solution of the half-taper angle adjustment.

To obtain the permanent angular velocity and lead, we first determine the path of the middle point of the driving pin using Formula (9). After that, we have to insert the intersection circles of the driving pin, which are given perpendicularly to the centerline of the driving pin along its $\overline{A'B'}$ length (Figure 3), from the circular path to the elliptical path. This means that the r_h radius differences must be determined between the proper elliptical radius and the circular radius at arbitrary points along the paths. Practically, r_h is the difference between the proper point pairs on the paths. The r_h radius difference is (Figure 4).

$$r_h(\varphi_1) = \frac{d_m}{2} \cdot \left[\frac{cos\varphi_1}{cos\delta_1 \cdot cos\left(sin^{-1}\sqrt{1 - \frac{cos^2\varphi_1}{cos^2\delta_1}} \right)} - 1 \right] \tag{17}$$

After the selection of an arbitrary point on the circular path, accordingly, (9) and (17), the x and r_h value pairs are determinable. The x and r_h chart in the function of φ_1 gives the modified center path of the driving pin along which the intersection circles can be swept (Figure 5). The shape is a curve that has to be determined for different geometries and manufacturing parameters. The diameter of the intersection circle is equal to the diameter

of the driving pin. The modified geometric configuration of the driving pin is shown in Figure 5.

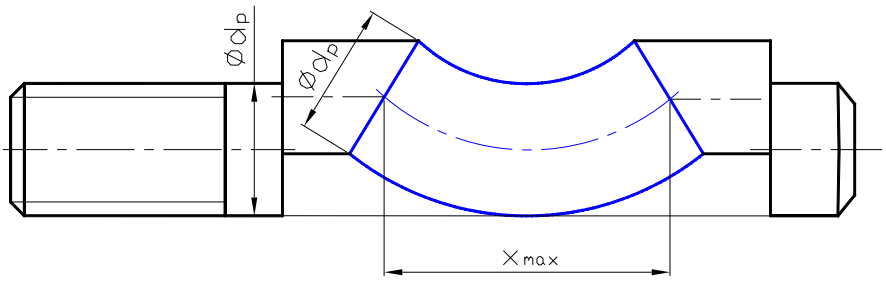

Figure 5. The modified geometric establishment of the driving pin.

The modified driving pin has to be fixed to the driver plate. During n_g number of revolutions, the driving pin and the lathe dog are in contact along the length of the x contact point displacement (Figure 6).

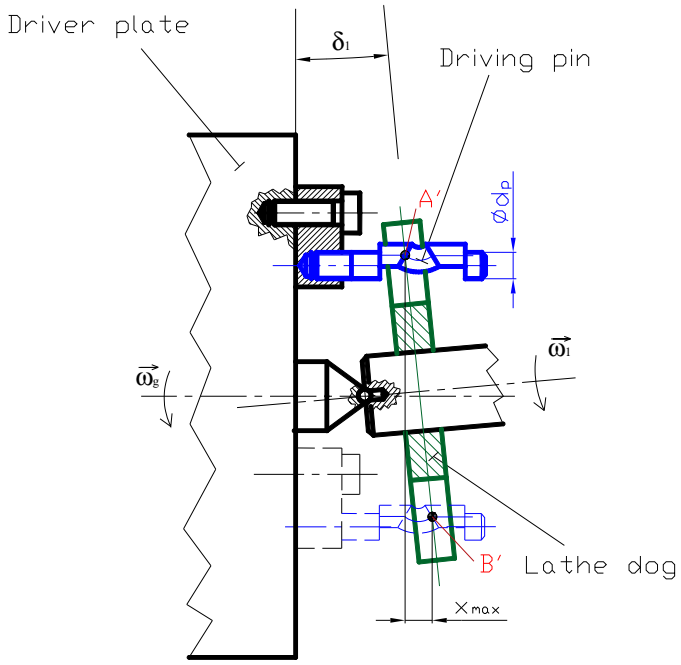

Figure 6. Application of the modified driving pin.

The r_h difference distances shown in Figure 4 represent the differences between the ellipse radius and the circular radius for a given point. This distance naturally varies from point to point along the circular path. Formula (17) gives how this distance can be calculated as a function of the angular displacement of the circular path (φ_1). The distance x shows the displacement of the contact points along the driving pin. In the case of a spiroid worm with a given geometry, the trajectory curve along which, by sweeping the circular cross-section of the applied driving pin, we obtain an optimized driving pin geometry can be determined as a function of the parameters x and r_h (Figures 5 and 6). That is, along the distance between the contact points x, the position of the circular cross-section of the driving pin point by point is changed according to the differences in r_h compared to the starting horizontal straight centerline. This changes the position of the contact point between the driving pin and the lathe dog not only horizontally but also in height. The radius differences r_h are exactly the radius differences of the corresponding circular and ellipse paths belonging to the given angular displacement points (φ_1). Thus, the trajectory

of the contact points of the driving pin and lathe dog, moving on an elliptical path curve modified by the adjustment of the spiroid worm with a half-cone angle, can be restored to the initial circular path, so that no radial fluctuation occurs as a result of the angular rotation, i.e., there will be no lead and angular velocity fluctuation errors.

2.4. Creation of the New-Type Mathematical Model

A new mathematical model is needed to determine the appropriate grinding wheel profile and analyze the overall grinding process kinematically (Figure 7).

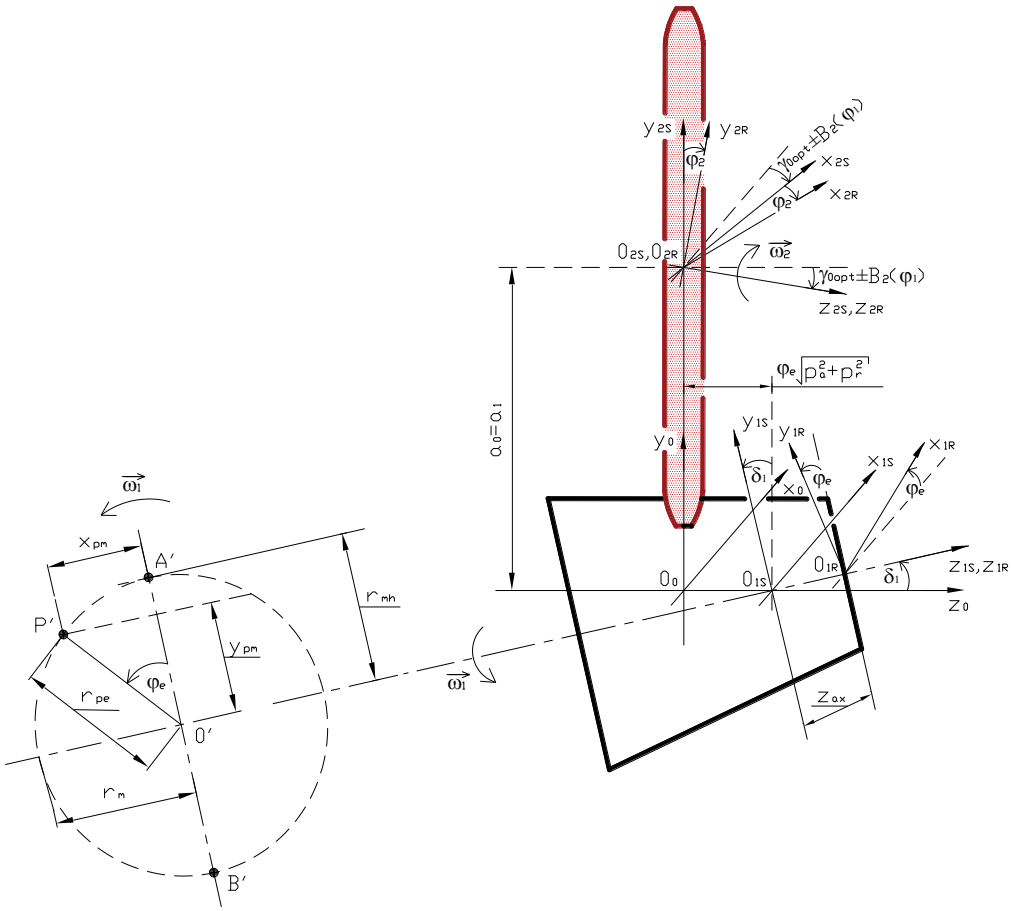

Figure 7. The new-type mathematical model.

The transformation matrixes between the coordinate systems are as follows (Figure 7):

$$\boldsymbol{M_{1S,1R}} = \begin{bmatrix} cos\left[sin^{-1}\left(\sqrt{1-\frac{cos^2\varphi_1}{cos^2\delta_1}}\right)\right] & -\sqrt{1-\frac{cos^2\varphi_1}{cos^2\delta_1}} & 0 & 0 \\ \sqrt{1-\frac{cos^2\varphi_1}{cos^2\delta_1}} & cos\left[sin^{-1}\left(\sqrt{1-\frac{cos^2\varphi_1}{cos^2\delta_1}}\right)\right] & 0 & 0 \\ 0 & 0 & 1 & z_{ax} \\ 0 & 0 & 0 & 1 \end{bmatrix} \quad (18)$$

$$\boldsymbol{M_{1R,1S}} = \begin{bmatrix} cos\left[sin^{-1}\left(\sqrt{1-\frac{cos^2\varphi_1}{cos^2\delta_1}}\right)\right] & \sqrt{1-\frac{cos^2\varphi_1}{cos^2\delta_1}} & 0 & 0 \\ -\sqrt{1-\frac{cos^2\varphi_1}{cos^2\delta_1}} & cos\left[sin^{-1}\left(\sqrt{1-\frac{cos^2\varphi_1}{cos^2\delta_1}}\right)\right] & 0 & 0 \\ 0 & 0 & 1 & -z_{ax} \\ 0 & 0 & 0 & 1 \end{bmatrix} \quad (19)$$

$$\boldsymbol{M_{0,1S}} = \begin{bmatrix} 1 & 0 & 0 & 0 \\ 0 & cos\delta_1 & -sin\delta_1 & 0 \\ 0 & sin\delta_1 & cos\delta_1 & sin^{-1}\left(\sqrt{1-\frac{cos^2\varphi_1}{cos^2\delta_1}}\right)\cdot\sqrt{p_a^2+p_t^2} \\ 0 & 0 & 0 & 1 \end{bmatrix} \tag{20}$$

$$\boldsymbol{M_{2S,0}} = \begin{bmatrix} cos(\gamma_{opt} \pm B_2) & 0 & sin(\gamma_{opt} \pm B_2) & 0 \\ 0 & 1 & 0 & -a_0 \\ -sin(\gamma_{opt} \pm B_2) & 0 & cos(\gamma_{opt} \pm B_2) & 0 \\ 0 & 0 & 0 & 1 \end{bmatrix} \tag{21}$$

$$\boldsymbol{M_{0,2S}} = \begin{bmatrix} cos(\gamma_{opt} \pm B_2) & 0 & -sin(\gamma_{opt} \pm B_2) & 0 \\ 0 & 1 & 0 & a_0 \\ sin(\gamma_{opt} \pm B_2) & 0 & cos(\gamma_{opt} \pm B_2) & 0 \\ 0 & 0 & 0 & 1 \end{bmatrix} \tag{22}$$

$$\boldsymbol{M_{2R,2S}} = \begin{bmatrix} cos\varphi_2 & -sin\varphi_2 & 0 & 0 \\ sin\varphi_2 & cos\varphi_2 & 0 & 0 \\ 0 & 0 & 1 & 0 \\ 0 & 0 & 0 & 1 \end{bmatrix} \tag{23}$$

$$\boldsymbol{M_{2S,2R}} = \begin{bmatrix} cos\varphi_2 & sin\varphi_2 & 0 & 0 \\ -sin\varphi_2 & cos\varphi_2 & 0 & 0 \\ 0 & 0 & 1 & 0 \\ 0 & 0 & 0 & 1 \end{bmatrix} \tag{24}$$

Knowing the (18)–(24) transformation matrixes, the transformation matrixes between rotating systems can be determined:

$$\boldsymbol{M_{1R,2R}} = \boldsymbol{M_{1R,1S}}\cdot\boldsymbol{M_{1S,0}}\cdot\boldsymbol{M_{0,2S}}\cdot\boldsymbol{M_{2S,2R}} \tag{25}$$

$$\boldsymbol{M_{2R,1R}} = \boldsymbol{M_{2R,2S}}\cdot\boldsymbol{M_{2S,0}}\cdot\boldsymbol{M_{0,1S}}\cdot\boldsymbol{M_{1S,1R}} \tag{26}$$

After the determination of the (25) and (26) transformation matrices, the purpose is to determine the necessary grinding wheel profile for the manufacturing of a given spiroid worm [2,3,7].

The position vector is given on the C_{1R} coordinate system, which is the equation of the spiroid worm [2,12]:

$$\vec{r_{1R}} = \vec{r_{1R}}(\eta,\ \vartheta) = \begin{bmatrix} x_{1R}(\eta,\ \vartheta) \\ y_{1R}(\eta,\ \vartheta) \\ z_{1R}(\eta,\ \vartheta) \\ 1 \end{bmatrix} \tag{27}$$

We intend to determine the wrapping surface that is connected to the $\vec{r_{1R}}(\eta,\ \vartheta)$; we can utilize the fact that the two surfaces wrap each other during mutual motions:

$$\varphi_2 = i_{21}\cdot sin^{-1}\left(\sqrt{1-\frac{cos^2\varphi_1}{cos^2\delta_1}}\right) \tag{28}$$

The plane that is defined by the $\frac{\partial\vec{r_{1R}}(\eta,\ \vartheta)}{\partial\eta}$ and $\frac{\partial\vec{r_{1R}}(\eta,\ \vartheta)}{\partial\vartheta}$ parameter lines is the tangent plane of the surface on a given point. The surface normal vector is perpendicular for the tangent plane [2,12]:

$$\vec{n_{1R}} = \frac{\partial\vec{r_{1R}}(\eta,\ \vartheta)}{\partial\eta} \times \frac{\partial\vec{r_{1R}}(\eta,\ \vartheta)}{\partial\vartheta} \tag{29}$$

The relative velocity between the two wrapping surfaces can be determined based on the transformation between the C_{1R} and C_{2R} systems on the C_{2R} system [2,12]:

$$\vec{v}_{2R}^{(1,2)} = \frac{d}{dt}\vec{r}_{2R} = \frac{d}{dt}(\boldsymbol{M_{2R,1R}})\cdot\vec{r}_{1R} \tag{30}$$

In order to determine the necessary wrapping surface, the $\vec{v}_{2R}^{(1,2)}$ vector has to be transformed into the C_{1R} system [2,12]:

$$\vec{v}_{1R}^{(1,2)} = \boldsymbol{M_{1R,2R}}\cdot\vec{v}_{2R}^{(1,2)} = \boldsymbol{M_{1R,2R}}\cdot\frac{d}{dt}(\boldsymbol{M_{2R,1R}})\cdot\vec{r}_{1R} = \boldsymbol{P_{1k}}\cdot\vec{r}_{1R} \tag{31}$$

where $\boldsymbol{P_{1k}}$ is the kinematic transformer matrix.

The contact line between the wrapping surfaces can be determined based on the Connection I statement [2,12]:

$$\vec{n}_{1R}\cdot\vec{v}_{1R}^{(1,2)} = \vec{n}_{2R}\cdot\vec{v}_{2R}^{(1,2)} = 0 \tag{32}$$

The developing surface of the connection line that is the surface of the grinding wheel is on the C_{2R} system [2,12]:

$$\left.\begin{array}{c}\vec{n}_{1R}\cdot\vec{v}_{1R}^{(1,2)} = 0\\ \vec{r}_{1R} = \vec{r}_{1R}(\eta,\ \vartheta)\\ \vec{r}_{2R} = \boldsymbol{M_{2R,1R}}\cdot\vec{r}_{1R}\end{array}\right\} \tag{33}$$

The $R_g = R_g(z_{2R})$ tool profile function is given if the received points are transformed into the tool axial plane of the grinding wheel [2,12]:

$$\left.\begin{array}{c}R_g = \sqrt{x_{2R}^2 + y_{2R}^2}\\ z_{2R} = z_{2R}(\eta,\vartheta)\end{array}\right\} \tag{34}$$

The mathematical model developed in this publication is based on the general mathematical model of Illés Dudás [2] and the mathematical model discussed in the PhD thesis in [3]. The general mathematical model of Dudás can be used for the geometric, mathematical, connection, and manufacturing technology analysis of worm drives with arbitrary geometry [2]. The model further developed in the Ph.D. dissertation found in [3] is suitable for the kinematic analysis of more accurate machining of the spiroid worm shaft with variable center distances and lead angle correction and for the determination of the grinding wheel profile optimized for profile accuracy from manufacturing aspects.

The model discussed in this publication is suitable for examining the angular velocity and lead fluctuations resulting from machining with a constant center distance while applying lead angle correction. By using the model, the grinding wheel profile optimized for profile accuracy from manufacturing aspects can be determined based on the principle of double-wrapping, with which the thread surface of the spiroid worm shaft can be produced.

3. Results

The main parameters for the manufacturing of the spiroid worm, with a concrete geometry examined, are presented in Table 1. The half-taper angle is modified to assess the effect of the received manufacturing parameters.

Table 1. The parameters in the manufacturing of the spiroid worm [4].

Name of the Parameter	Value
The highest tip circle diameter (d_{amax})	73.87 mm
The highest pitch circle diameter (d_{pmax})	72.998 mm
Half-taper angle (δ_1)	2° 4° 5° 6° 7° 8° 9° 10°
Whole depth (h_w)	11.25 mm
Radial increment parameter (p_r)	0.218722 mm/radian
Axial increment parameter (p_a)	2.5 mm/radian
Worm length (l)	73 mm
Axial lead (H)	15.708 ± 0.015 mm
Total length of the spiroid worm shaft (L)	482 mm
The diameter of the circular path of the driving pin (d_m)	100 mm
The external diameter of the applied grinding wheel (d_{agw})	400 mm
The eccentricity distance (e) based on Formula (8)	41.988 mm
The number of revolutions of the spindle (n_g)	45 1/min
The angular velocity of the driving pin on the pitch circle ($\vec{\omega_g}$) based on Formula (1)	4.71 1/min

All of the determined Formulas (1)–(18) were programmed in Microsoft Excel to determine the necessary manufacturing parameters and to analyze the effect of the modification of the half-taper angle on the spiroid worm, assuming constancy of the other initial geometric and manufacturing parameters (Table 1).

The angular displacement and the lead error can be seen in Figure 8. The shape of the functions is an approximately sinusoidal form, which means error fluctuations in the function of the angular displacement. This fluctuation is determined for different half-taper angles, as shown in Table 1. The fluctuations are within the prescribed tolerance zone (Table 1) under 9°.

In contrast, the prescribed tolerances cannot be maintained for 9 ° or 10° half-taper angles (Figure 8); therefore, the new-type driving pin must be used, which has different curves.

The function of the angular displacement and the angular velocity on the elliptical path ($\vec{\omega_1}$) can be seen in Figure 9 compared to the permanent angular velocity.

The shapes of the functions are approximately the same as the shape of the sine function.

The function of the path of the driving pin (x) and the radius distances between the ellipse and the circular paths (r_h) can be seen in Figure 10, which is the curve of the intersection circle on the driving pin. The figures' shapes are similar to those of the parabola. The calculated results are almost identical for 2° and 4° half-taper angles. This is why the results for a 4° half-taper angle are not shown. Based on the diagram, the length of the curve increases with the increase in the half-taper angle (Figure 10).

Lagrange interpolation is used to determine the geometric equations of the optimized curves of the driving pin to eliminate the lead error and the fluctuation of the angular velocity in case of different half-taper angles (Table 2).

Table 2. The Lagrange equations for different half-taper angles.

Half-Taper Angle	Lagrange Equation	
2°	$r_h = 0.001 \cdot x^2 - 0.03489 \cdot x + 0.03044$	(35)
5°	$r_h = 0.00998 \cdot x^2 - 0.08726 \cdot x + 0.19082$	(36)
6°	$r_h = 0.00997 \cdot x^2 - 0.10473 \cdot x + 0.27519$	(37)
7°	$r_h = 0.00996 \cdot x^2 - 0.122223 \cdot x + 0.37523$	(38)
8°	$r_h = 0.00995 \cdot x^2 - 0.13974 \cdot x + 0.49109$	(39)
9°	$r_h = 0.00994 \cdot x^2 - 0.15727 \cdot x + 0.62289$	(40)
10°	$r_h = 0.00992 \cdot x^2 - 0.17482 \cdot x + 0.7711$	(41)

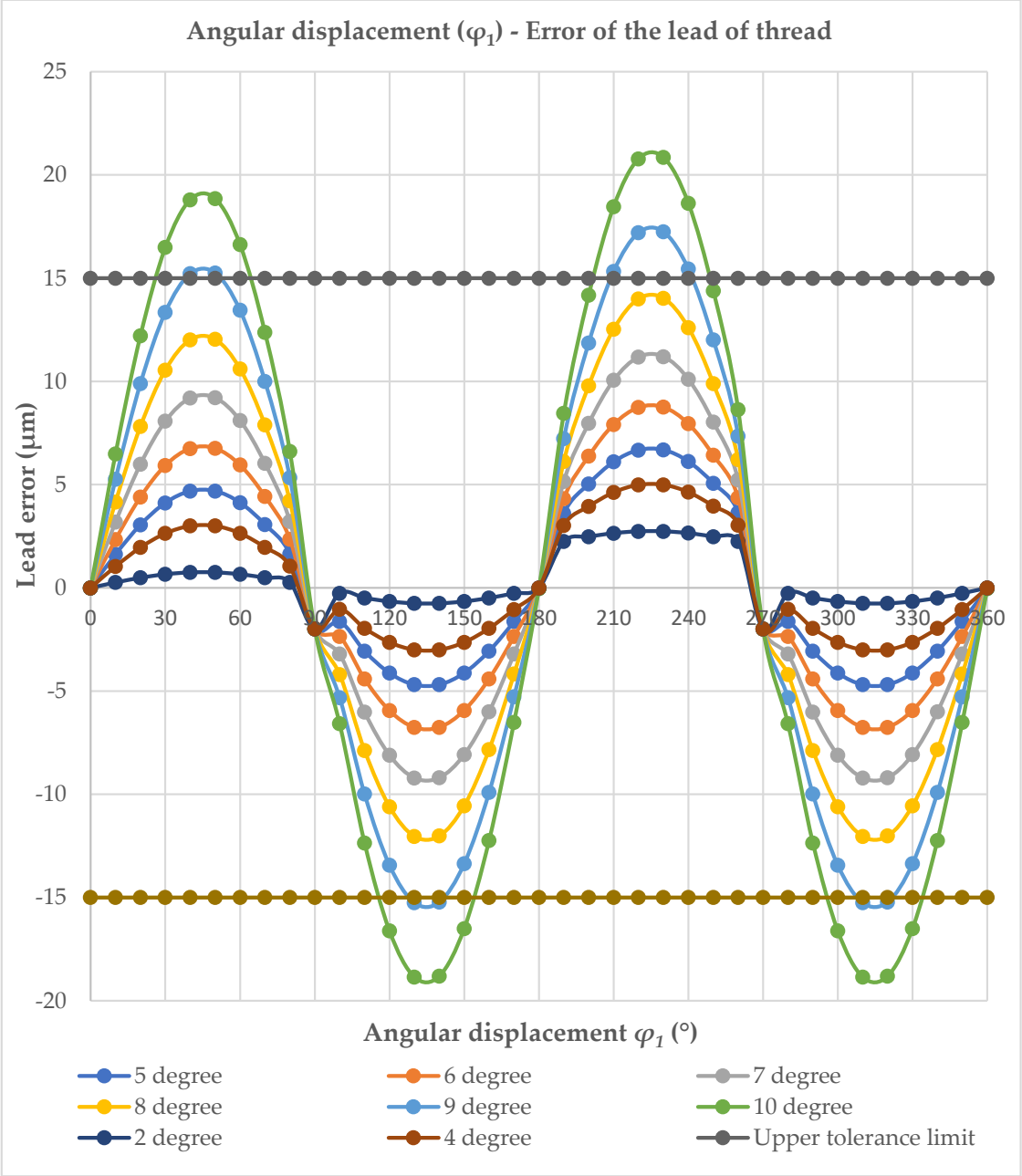

Figure 8. The function of the angular displacement and the lead error.

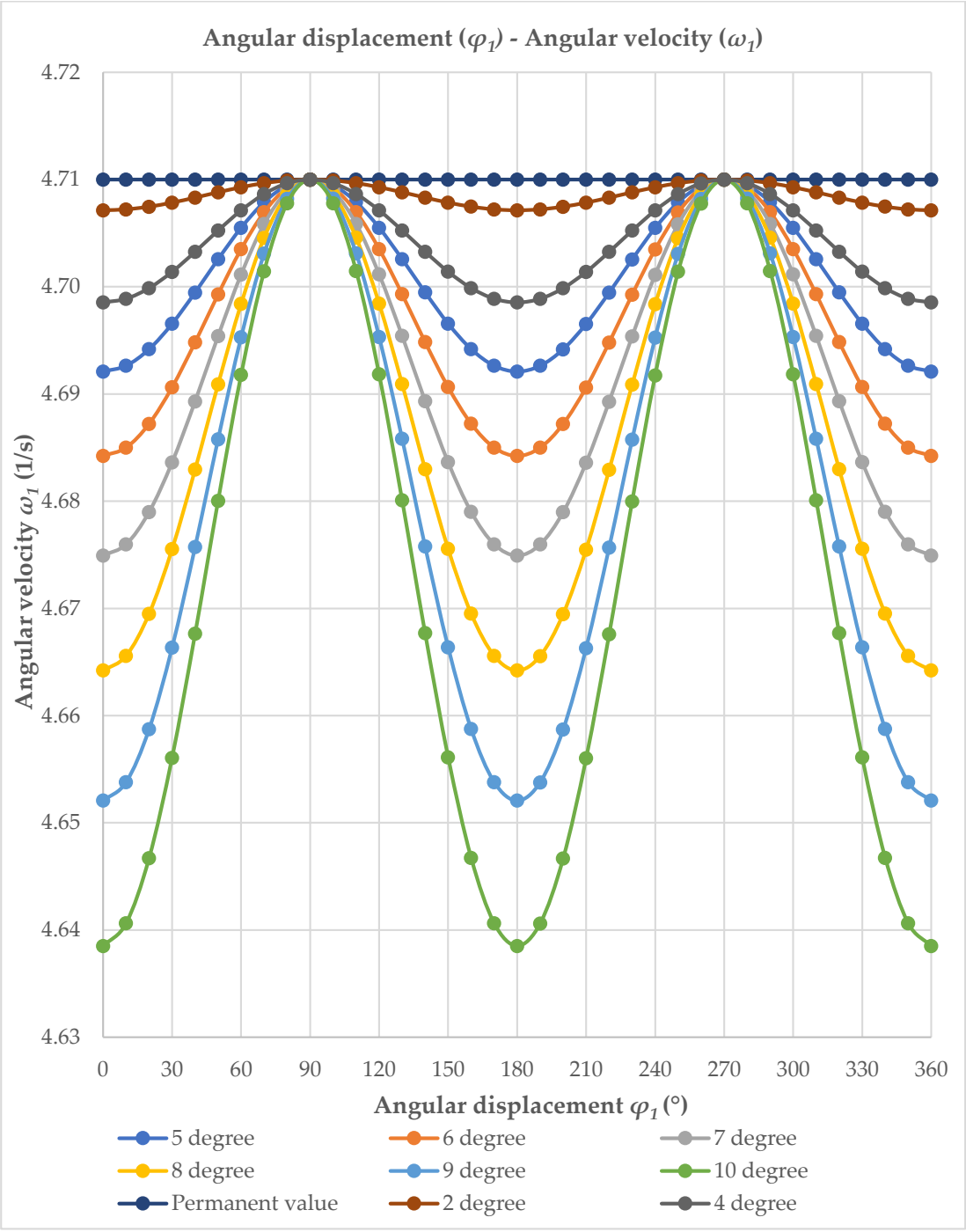

Figure 9. The function of the angular displacement and the angular velocity on the elliptical path.

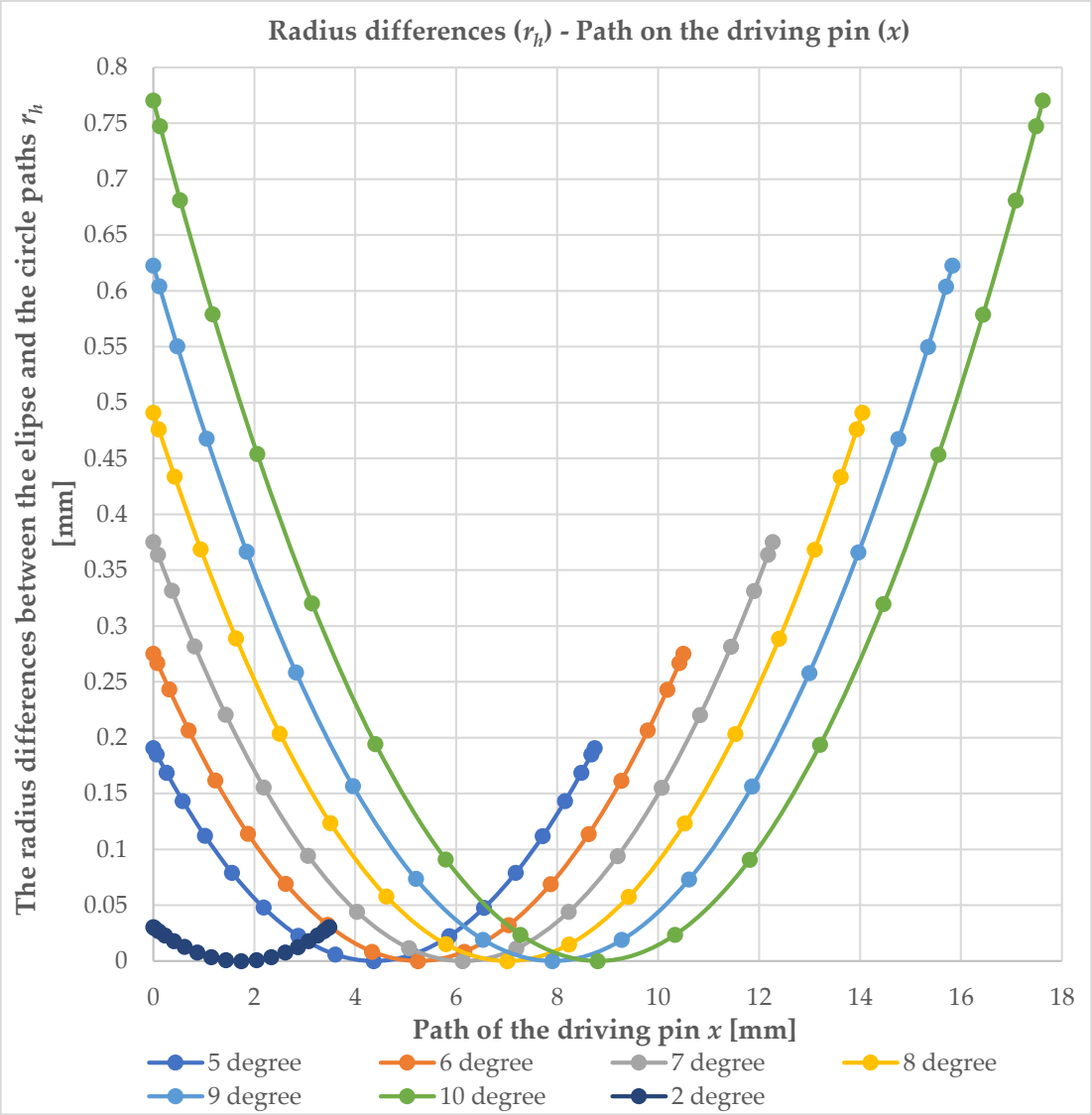

Figure 10. The function of the path of the driving pin and radius differences between the paths.

4. Discussion

We analyzed the grinding technology of the spiroid worm shaft on a classical working machine, in which the worm shaft is offset by the half-taper angle. During production, lead angle correction is applied when the grinding wheel is rotated. The grinding wheel profile is determined using the optimal wheel profile determination algorithm developed by Professor Illés Dudás [2]. A mathematical model was developed for a detailed analysis of the manufacturing process.

The wheel profile is controlled by a CNC-controlled wheel regulation device. A new grinding wheel tilting spindle housing is used to ensure the wheel lead angle correction is applied during CNC-controlled machining. Of course, the grinding wheel rotates at a constant peripheral speed during the manufacturing process.

We have determined the necessary correlations and formulas for the analysis and design of this manufacturing technology.

Since the teeth of the spiroid worm are asymmetrical, the grinding process must be carried out twice for a spiroid worm, i.e., for the low and high sides [10].

For a spiroid worm shaft with a specific geometry, we analyzed the manufacturing parameters, accounting for the given driving pin and its circular path.

We varied the half-taper angle of the spiroid worm while holding the other initial geometric parameters constant to determine the correlation between the manufacturing parameters and the half-taper angle modification. We determined the change in the lead error and the change in the angular velocity along the elliptical path as a function of the spindle angular displacement for different half-taper angle values of the spiroid worm.

We determined the path of the contact points along the length of the driving pin during engagement with the lathe dog.

We have determined the radial differences between the corresponding points on the elliptical and circular paths. Based on the radius differences, the geometry of the driving pin can be modified to solve the fluctuation in lead error and the variable angular velocity. If we plot the trajectory of the contact points—the radius difference function—we get a curve. If we draw the radial circle section (intersection circle) of the driving pin along the resulting curve, we get the geometric shape with which the angular velocity and the lead error fluctuations can be eliminated while the driving pin is rotated.

We have presented the modified driving pin geometry in a general case. Using Lagrange interpolation, we have determined the equations of the curves obtained on the driving pin, facilitating further mathematical analyses, the driving pin CAD modeling process, and CNC manufacturing design. This driving pin with a new geometry can be manufactured using CNC technology or additive manufacturing using metal powder.

The grinding method described in this publication can be applied to different spiral worm or hob geometries with different starting manufacturing cases.

4.1. Substantive and Critical Analysis of the Results

The results indicate that the developed mathematical model and the modified driving pin geometry may be suitable for reducing lead error and angular velocity fluctuations, thereby improving the manufacturing accuracy of spiroid worms. It is noteworthy that the effect of varying the half-taper angle was analyzed quantitatively, and a specific geometric correction method was identified to compensate for manufacturing errors.

However, the analysis is primarily theoretical and simulation-based, and it is not clearly demonstrated to what extent the proposed solutions are valid in experimental or industrial environments. Furthermore, the sensitivity of the model to input parameters and aspects of practical applicability (such as manufacturing costs and implementation complexity) are not examined in detail, which limits the direct industrial applicability of the results.

4.2. Limitations of This Research

This research provides many important results for the analysis and development of spiroid worm shaft grinding technology, but it also has certain limitations that must be considered when interpreting and applying the results in practice.

The tests are primarily based on a machining model performed on a classic cylindrical grinding machine, in which the worm shaft is adjusted by the half-taper angle. This approach assumes that the manufacturing environment is ideal and well-controlled, so that deviations from real industrial conditions (such as vibrations, thermal effects, or machine geometric inaccuracies) are not taken into account in detail.

The mathematical model and the relationships derived from it are deterministic and do not contain stochastic or uncertainty factors. As a result, the accuracy of the model may be limited in cases where random errors or inhomogeneities in material properties occur during the manufacturing process.

During these studies, several geometric parameters were considered constant, while only the effect of varying the half-taper angle was analyzed. This simplifies the analysis but,

at the same time, limits the generalizability of the results to other geometric configurations, where simultaneous changes in several parameters can have a significant impact on the manufacturing process.

Due to the asymmetry of the spiroid gear teeth, the grinding process must be performed in two separate steps (low- and high-side grinding), which increases the technological complexity. This research takes this into account; however, a detailed examination of the cumulative defects resulting from double-sided machining is not the subject of this analysis.

The modified geometry of the driving pin is determined based on the radial deviations between the elliptical and circular paths and is based on ideal geometric assumptions. In practice, manufacturing and assembly inaccuracies, as well as the effects of wear, can affect the actual contact conditions, which can cause deviations from the theoretical results.

Furthermore, although this study proposes CNC or additive manufacturing of the modified driving pin, it does not analyze in detail the impact of differences in accuracy, surface quality, and material structure resulting from different manufacturing technologies.

Finally, the generalizability of the presented method to other thread surfaces or hob geometries is formulated at a theoretical level. However, its experimental validation is not part of this research; thus, its practical applicability requires further investigations.

4.3. Future Research Directions

Building on the results of the presented research, several future research directions can be identified that could further increase the accuracy, efficiency, and industrial applicability of the manufacturing technology of spiroid worm shafts.

One of the most important directions is to further develop the mathematical model, especially taking into account real production conditions. It would be worthwhile to incorporate stochastic effects, such as machine vibrations, thermal deformations, and dynamic changes in tool wear, into the model. This would allow for the development of a more robust predictive model that can be reliably applied in an industrial environment.

Another research opportunity is the investigation of multi-parameter optimization. The current analysis primarily focuses on the effect of the half-taper angle; however, the effect of changing geometric and technological parameters (e.g., feed, speed, tool profile, and cooling conditions) together can result in complex interactions. By applying multivariable optimization methods, manufacturing accuracy and surface quality could be further improved.

It is also of utmost importance to extend the experimental validation. Practical testing of the proposed theoretical relationships and modified driving pin geometries on different machines and manufacturing environments would help to verify the generalizability of the results and to reveal any possible deviations.

It would also be worth investigating the integration of modern manufacturing technologies. For example, the use of additive manufacturing may offer new possibilities for the production of complex driving pin geometries, but its impact on mechanical properties, wear resistance and service life still requires further research. Similarly, hybrid manufacturing processes (additive + machining) may also be a promising direction.

The development of CNC control is also an important area of research. The development of adaptive, real-time control algorithms may enable immediate compensation of manufacturing errors, for example by using sensor data (vibration, force, and temperature). This may be particularly important in minimizing errors resulting from asymmetric gearing.

Another direction is the study of wear and service life. An analysis of the long-term behavior of the grinding wheel and the modified driving pin can contribute to the optimization of maintenance strategies and a reduction in production costs.

Finally, it would be useful to extend the method to different worm and hob types, as well as to different industrial applications. In doing so, not only geometric but also tribological and load aspects should be taken into account, so that the developed technology can be applied more widely.

Together, these directions can contribute to the development of a more intelligent, adaptive and higher-precision manufacturing system in the field of spiroid drives.

5. Conclusions

This publication analyses the grinding of a spiroid worm using lathe center displacement, a constant center distance, and lead angle correction. Lathe center displacement is applied to align the worm's taper generation to a horizontal angular position, ensuring a constant center distance between the grinding wheel and the workpiece.

Due to the displacement, the worm follows an elliptical path instead of a circular one, resulting in non-constant angular velocity and, consequently, lead errors during grinding. To address this, a mathematical model is developed for the kinematic analysis of the process and for determining the optimal grinding wheel profile based on the mutual wrapping principle of the worm and wheel surfaces.

Because the pitch circle diameter and lead angle vary along the tapered worm, an optimal wheel inclination angle is determined using the method of Professor Illés Dudás. The final wheel profile is obtained from the smallest and largest pitch circle diameters, and their average is used to define the optimal geometry. During machining, continuous lead angle correction is applied to improve accuracy by tracking changes in the thread lead in real time.

This study also investigates fluctuations in lead error and angular velocity, leading to an optimized driving pin geometry that minimizes these deviations and keeps the worm profile within tolerance limits.

Although this work is theoretical, it has strong industrial relevance. However, practical implementation would require significant investment in CNC equipment and advanced measurement systems (e.g., CCD-based or sensor-equipped monitoring), which currently limits experimental validation.

Overall, the proposed method improves grinding accuracy by combining precise kinematic modeling, optimized tool geometry, and continuous lead correction, offering a robust approach for high-quality spiroid worm manufacturing, albeit with high equipment demands.

5.1. Specific Advantage

One of the most important advantages of this method is that, through continuous lead angle correction and optimized driving pin geometry, it significantly reduces profile errors and inaccuracies caused by non-uniform angular velocity, thereby improving the grinding accuracy of the spiroid worm and the quality of the final tooth profile.

5.2. Specific Limiting Factor

A major limitation of practical implementation is the high investment requirement, as the method can only be realized using a specialized CNC machine tool and advanced measurement systems (e.g., CCD cameras or sensor-based monitoring). This significantly complicates both industrial application and experimental validation at present.

Author Contributions: Conceptualization: S.B.; Methodology: S.B.; software: G.S., validation: G.S. and T.L.; formal analysis: G.S. and T.L.; writing—original draft preparation: S.B.; writing—review and editing: G.S. and T.L. All authors have read and agreed to the published version of the manuscript.

Funding: This research received no external funding.

Data Availability Statement: The original contributions presented in this study are included in the article. Further inquiries can be directed to the corresponding author.

Conflicts of Interest: The authors declare no conflict of interest.

Appendix A

Symbol	Name	Unit
$\vec{n}_{1R}$	Unit normal vector of a helicoidal surface in the C_{1R} coordinate system	
$\vec{n}_{2R}$	Unit normal vector of a helicoidal surface in the C_{2R} coordinate system	
$\vec{r}_{1R}$	Position vector of the generating curve of a spiroid worm surface	
$\vec{r}_{2R}$	Position vector of a moving point of the grinding wheel surface	
$\vec{v}_{1R}^{(1,2)}$	Velocity vector of the helicoid and grinding wheel surfaces in the C_{1R} coordinate system	[m/min]
$\vec{v}_{2R}^{(1,2)}$	Velocity vector of the helicoid and grinding wheel surfaces in the C_{2R} coordinate system	[m/min]
$\vec{v}_g$	Circumferential speed of the spindle	[mm/min]
$\vec{\omega}_1$	Angular velocity around the elliptical path	[1/min]
$\vec{\omega}_2$	Angular velocity of the grinding wheel	[mm]
$\vec{\omega}_g$	Angular velocity of the spindle around the circular path	[1/min]
γ_o	Lead angle on an arbitrary pitch diameter	[°]
γ_{opt}	Optimized lead angle	[°]
$\pm B_2$	Lead angle correction	[°]
a, b, c	The positioning distances required to connect the spiroid worm and the face gear	[mm]
A, B, P	Selected points on the circular path	
A', B', P'	Corresponding points on the elliptical path	
$a_0 = a_1$	Elementary center distance between the spiroid worm and the grinding wheel	[mm]
C_0 (x_0, y_0, z_0)	Stationary coordinate system fixed to the working machine	
C_{1R} (x_{1R}, y_{1R}, z_{1R})	Rotating coordinate system fixed to a helicoidal surface	
C_{1S} (x_{1S}, y_{1S}, z_{1S})	Standing coordinate system connected to the linear table of the working machine	
C_{2R} (x_{2R}, y_{2R}, z_{2R})	Rotating coordinate system fixed to a grinding wheel	
C_{2S} (x_{2S}, y_{2S}, z_{2S})	Stationary coordinate system fixed to a grinding wheel	
CAD	Computer-aided design	
CAM	Computer-aided manufacturing	
d_{agw}	External diameter of the grinding wheel	[mm]
d_{amax}	Highest tip circle diameter of the spiroid worm	[mm]
d_m	Diameter of the circular path	[mm]
d_{mh}	The minor axis of the elliptical path	[mm]
e	Peak adjustment distance	[mm]
H	Axial lead of the thread	[mm]
h_{a1}	Addendum of the spiroid worm	[mm]
h_w	Whole depth	[mm]
i_{21}	Gear transmission ratio	
l	Spiroid worm length	[mm]
L	Total length of the spiroid worm shaft	[mm]
$M_{0,1S}$	Coordinate transformation matrix (transforms C_{1S} to C_0)	
$M_{0,2S}$	Coordinate transformation matrix (transforms C_{2S} to C_0)	
$M_{1R,1S}$	Coordinate transformation matrix (transforms C_{1S} to C_{1R})	
$M_{1R,2R}$	Coordinate transformation matrix (transforms C_{2R} to C_{1R})	

Symbol	Name	Unit
$M_{1S,0}$	Coordinate transformation matrix (transforms C_0 to C_{1S})	
$M_{1S,1R}$	Coordinate transformation matrix (transforms C_{1R} to C_{1S})	
$M_{2R,1R}$	Coordinate transformation matrix (transforms C_{1R} to C_{2R})	
$M_{2R,2S}$	Coordinate transformation matrix (transforms C_{2S} to C_{2R})	
$M_{2S,0}$	Coordinate transformation matrix (transforms C_0 to C_{2S})	
$M_{2S,2R}$	Coordinate transformation matrix (transforms C_{2R} to C_{2S})	
n_g	Number of revolutions of the spindle	[1/min]
O	Origin of the circular path	
O'	Origin of the elliptical path	
O_0, O_{1S}, O_{1R}, O_{2S}, O_{2R}	Origins of coordinate systems related to their subscripts	
P_{1k}	Kinematic transformer matrix	
p_a	Axial increment parameter	[mm/radian]
p_r	Radial increment parameter	[mm/radian]
r_e	The changing radius on the elliptical path	[mm]
r_{ep}	Radius of the arbitrary selected P' point on the elliptical path	[mm]
R_g	Radius of the grinding wheel	[mm]
r_h	Radius distance between the proper elliptical radius and the circular radius	[mm]
r_{hmax}	Maximum radius distance	[mm]
r_{hp}	Radius distance that belongs to the P and P' points	[mm]
r_m	Radius of the circular path	[mm]
r_{mh}	Radius of the minor axis of the elliptical path	[mm]
x	Contact point displacement	[mm]
x_{max}	Maximum contact point displacement	[mm]
x_{pm}	Horizontal distance of the P' point on the elliptical path	[mm]
y_p	Vertical height of the P selected point on the circular path	[mm]
y_{pm}	Vertical distance of the P' point on the elliptical path	[mm]
z_{ax}	Axial translation of the helicoidal surface to the manufacturing position	[mm]
δ_1	Half-taper angle of a spiroid worm	[°]
η, ϑ	Internal parameters of the helicoidal surface	
φ_1	Angular displacement on the circular path	[°]
φ_e	Angular displacement on the elliptical path	[°]

References

1. Evertz, F.; Gangireddy, B.; Mork, B.; Porter, T.; Quist, A. Spiroid High Torque Gearing, 2021 High Torque Skew Axis Gearing, A Technical Primer, p. 19. Available online: https://www.spiroidgearing.com/wp-content/uploads/2019/05/Spiroid-Technical-Paper_Final.pdf?utm_source=chatgpt.com (accessed on 29 April 2026).
2. Dudás, I. *The Theory and Practice of Worm Gear Drives*; Penton Press: London, UK, 2000.
3. Balajti, Z. Development of Manufacturing Geometry of Kinematic Gear Pairs. Ph.D. Dissertation, University of Miskolc, Miskolc, Hungary, 2007. Available online: https://doktori.hu/doktori-vedesek/717/ (accessed on 29 April 2026).
4. Bodzás, S. Analysis of the Connection of Spiroid Worm, Face Gear, and Tool Surfaces. Ph.D. Dissertation, University of Miskolc, Miskolc, Hungary, 2014; p. 154.
5. Dudás, I.; Bodzás, S.; Dudás, I.S.; Mándy, Z. Spiroid Worm Pair with Concave Thread Profile and Method for Its Production by Grinding. P1200405, 4 July 2012. Available online: https://epub.sztnh.gov.hu/e-kutatas/ (accessed on 29 April 2026).
6. Dudás, I.; Bodzás, S.; Dudás, I.S.; Mándy, Z. Development of spiroid worm gear drive having arched profile in axial section and a new technology of spiroid worm manufacturing with lathe center displacement. *Int. J. Adv. Manuf. Technol.* **2015**, *79*, 1881–1892. [CrossRef]
7. Bodzás, S. Analysis of grinding technology of spiroid worm on a classical grinding machine. *Key Eng. Mater.* **2025**, *1019*, 3–12. [CrossRef]

8. Mándy, Z. Intelligent Manufacturing System for Spiroid Surfaces and Their Geometrically Accurate Machining. Ph.D. Dissertation, University of Miskolc, Miskolc, Hungary, 2022; p. 106. Available online: https://doktori.hu/doktori-vedesek/25163/ (accessed on 29 April 2026).
9. Dudás, L. Solving Manufacturing Geometry Tasks of Mating Surface Pairs Based on the Reach Model. Candidate Dissertation, TMB, Budapest, Hungary, 1991; p. 144.
10. Bohle, F. Spiroid gears and their characteristics machinery. *Machinery Magazine*, 6 January 1956.
11. Radzevich, S.P. *Dudley's Handbook of Practical Gear Design and Manufacture*, 3rd ed.; CRC Press: Boca Raton, FL, USA, 2016; p. 615.
12. Litvin, F.L.; Fuentes, A. *Gear Geometry and Applied Theory*, 2nd ed.; Cambridge University Press: Cambridge, UK, 2004; p. 795.
13. Goldfarb, V.; Trubachev, E.; Barmina, N. *Advenced Gear Engineering*; Mechanisms and Machine Science 51; Springer: Berlin/Heidelberg, Germany, 2018; p. 495.
14. Goldfarb, V.; Barmina, N. *Theory and Practice of Gearing and Transmissions*; In honor of Professor F. L. Litvin, Mechanisms and Machine Science 34; Springer: Berlin/Heidelberg, Germany, 2016; p. 425.
15. Goldfarb, V.; Trubachev, E.; Barmina, N. Innovations in Design and Production of Spiroid Gears in the XXI Century. In Proceedings of the 6th International BAPT Conference "Power Transmissions 2019", Varna, Bulgaria, 19–22 June 2019; Volume 287, p. 7. [CrossRef]
16. Goldfarb, V.I.; Trubachev, E.S.; Bogdanov, K.V.; Pushkareva, T.A. Prospects of manufacturing spiroid gears with small gear ratios. *Forsch. Im Ingenieurwesen* **2019**, *83*, 781–791. [CrossRef]
17. Trubachev, E.; Bogdanov, K.; Pushkareva, T. Advanced method of cutting spiroid, worm and bevel gearwheel teeth by running-in cutter heads. *Forsch. Im Ingenieurwesen* **2022**, *86*, 709–719. [CrossRef]
18. Tkachuk, A.; Ignatyugin, V. Grinding the side surfaces of the spiroid cylindrical gear worm turns with a tapered wheel. In Proceedings of the International Scientific Siberian Transport Forum—TransSiberia 2023, Novosibirsk, Russia, 28–30 June 2023; Volume 402. [CrossRef]
19. Trubachev, E. Spiroid gears as an alternative to bevel and hypoid gears. In *Proceedings of the 9th International Conference on Industrial Engineering. ICIE 2023, Sochi, Russia, 15–19 May 2023*; Radionov, A.A., Gasiyarov, V.R., Eds.; Lecture Notes in Mechanical Engineering; Springer: Cham, Switzerland, 2023. [CrossRef]
20. Staniek, R. Shaping of the face worm gear by means of the single edge cutting tool. In *Proceedings of the ASME 2008 9th Biennial Conference on Engineering Systems Design and Analysis. Volume 1: Advanced Energy Systems; Advanced and Digital Manufacturing; Advanced Materials; Aerospace, Haifa, Israel, 7–9 July 2008*; ASME: New York, NY, USA, 2008; pp. 247–253. [CrossRef]
21. Trubachev, E.; Barmina, N. Innovations in design of worm-type gears in the last two decades. In *State-of-the-Art and Innovations in Mechanism and Machine Science*; Ceccarelli, M., Jauregui-Correa, J.C., Eds.; Mechanisms and Machine Science; Springer: Berlin/Heidelberg, Germany, 2024; Volume 150. [CrossRef]
22. Zhang, X.-C.; Nie, J.-H. Double lead spiroid worm gearing with a beeline contact, II—The Ways of Cutting Tooth Surfaces. *J. Beijing Univ. Technol.* **2011**, *37*, 494–500.